Monitoring of Norilsk TPP-3 fuel tanks dynamics using Sentinel-1 SAR data

Monitoring of Norilsk TPP-3 fuel tanks dynamics using Sentinel-1 SAR data

A Zakharov and L Zakharova

V. A. Kotelnikov Institute of Radioengineering and Electronics RAS, Fryazino Branch
Vvedensky square, 1, Fryazino, Moscow region, 141190, Russian Federation

aizakhar@ire.rssi.ru

Abstract. The results of interferometric processing and analysis of European spaceborne synthetic aperture radar (SAR) Sentinel-1 acquired over the territory of Norilsk thermal power plant TPP-3 are presented. Radar interferograms created cover both cold season of 2019-2020 and warm season of 2020 including catastrophic event - the rupture of the tank with diesel fuel. Owing to high temporal stability of radar signals backscatter from the surface of TPP-3 territory on the time interval between repeated observations the monitoring of the stability of fuel tanks and adjacent territory using classical radar interferometry technique was conducted. It was discovered that the relative location of all four TPP-3 reservoirs and adjacent territory is stable within the 2-3 mm band on all the observation intervals. We may suppose that the fuel tank rupture was not caused by the dynamics of the study area as a consequence of permafrost thaw.

1. Introduction

According to the environmental consequences, the diesel fuel leakage at the TPP-3 fuel storage facility of the city of Norilsk on May 29, 2020 became a disaster of federal scale [1]. About 21 thousand tons of diesel fuel got into surrounding soil and water because of the depressurization of the fourth fuel storage tank. One of the main official versions of the accident reasons is that the thawing of frozen ground due to abnormally warm weather might damage the supports of the platform with fuel reservoirs.

Continuous permafrost is typical for the Norilsk region. Mostly typical soils here are tundra gley soils as well as boggy and alluvial soils. TPP-3 is located on the boundary of Nadezhda plateau. It adjoins the B.I. Kolesnikov metallurgical plant from the south-west as a part of the unified industrial zone.

This study aims at demonstration of the potential of spaceborne SAR interferometry (InSAR) in the detection of the subsidence of the scattering surface of the industrial zone near the reservoirs and/or horizontal displacements of the reservoirs walls. SAR interferometric observations from a satellite's repeated orbits as a tool allowing the detection of small-scale displacements of the scattering surfaces during the time interval between the radar observations has proven its efficiency in many applications of Earth remote sensing techniques [2-7]. Besides the natural surface changes, InSAR methods can be applied to the detection and monitoring of man-made objects, i.e., buildings, dams, industrial infrastructure and bridges [8-10].

2. Data set and observation geometry

InSAR technique is based on the conduction of repeated synthetic aperture radar observations from the same orbit of satellite platform. Sentinel-1 C-band SAR (wavelength 5.6 cm) of European Space Agency with 12 days repeat observations interval is among the best instruments and data sources for a given study. Analysis of Sentinel-1 SAR data availability in Copernicus archive (see https://scihub.copernicus.eu/dhus/#/home) shows that till June 2020 the TPP-3 area was imaged by Sentinel-1B satellite from the descending obit in the right-side direction of observation with 41° observation angle. Sentinel-1A few additional surveys were made in the same observation geometry also in early June 2020. Sentinel-1A orbital parameters provide the possibility to combine its data with Sentinel-1B in interferometric pairs with 6 days repeat observations interval. On the Google Earth picture in figure 1 yellow arrow marks the direction of the satellite flight path, and SAR observation direction is shown with broad arrow. Because of the reservoirs observation from eastern direction their western walls and small area nearby are shadowed. Accordingly, the damaged portion of the reservoir wall with fuel leakage location (white arrow in figure 1) is unseen.

Figure 1. Image of TPP-3 area and geometry of Sentinel-1 SAR observation from descending orbit.

Diesel fuel tanks in figure 1 are cylindrical structures 40 meters in diameter with cone-shaped roofs; they are spaced at 70 meters distance. Slope of the roofs does not exceed 20°. Radar images of such a structures with surfaces looking smooth in the signal wavelength scale differ from regular optical images. The dominating mechanism of the signal scattering from the tank walls and roof is mirror-like scattering. As a result, echo-signal of the roof will be scattered sideways from radar. Mirror-like scattering of the roof may be confirmed by the fact that after the roof deformation on May 29 the radar signature of the damaged tank was not changed. At the same time, vertical walls of the tank constitute diplane corner reflector with horizontal surface of the surrounding industrial zone. For that reason in a double-bounce scattering scheme radar signal arrives back to radar (see figure 2).

A specificity of the signal reflection by dihedral corner is the equality of the path length for all the rays falling on the edges. As a result, 20 meters high tank looks like bright point target located at the point C of the corner on the radar image with 2.3 m slant range resolution (see image fragment in upper right corner of figure 2). Small-scale displacements of vertical edge in horizontal direction or horizontal edge in vertical direction will led to the displacement of the corner top C and, consequently, alteration of the distance from radar.

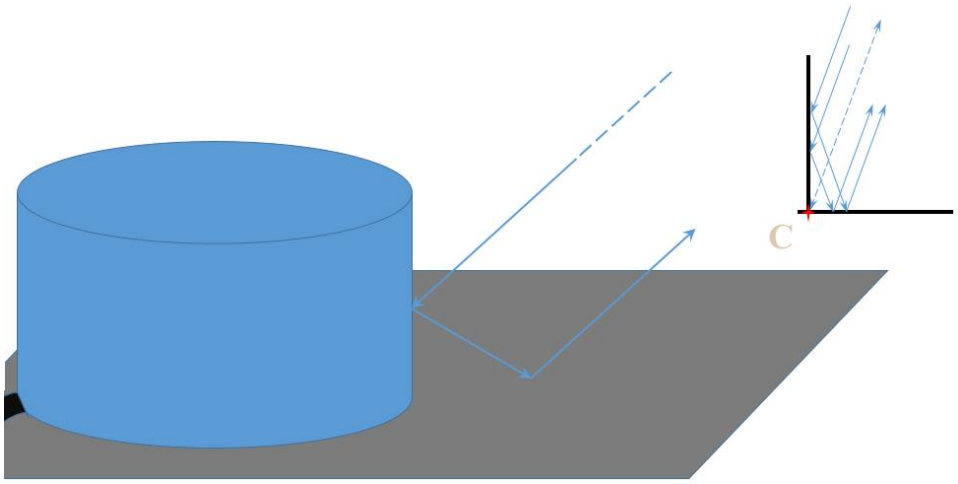

Figure 2. Interaction of radio waves with the reservoir construction.

3. Data processing and discussion

Level-1 Single Look Complex images acquired in Interferometric Wide mode of Sentinel-1 SAR sensor were used in the study. Each image pixel is represented by a complex (I and Q) magnitude value and therefore contains both amplitude and phase information. Slant range distance between pixels of the images is 2.3 m, and the distance between adjacent image lines in azimuth is 14.1 m. In order to reduce noise and to get almost equal surface resolution in range and azimuth an incoherent averaging of the interferogram in four pixels slant range window was applied. Non-linear filtering of interferogram with Goldstein filter having effective window size 5x5 pixels was made also. Topographic phase on interferogram was estimated using GMTED digital elevation model and removed, so the remaining phase variations characterize signal propagation path variations, for example, scattering surfaces displacement in slant range direction. Theoretical estimation of the interferometric phase measurements accuracy may be derived from the level of interferometric coherence of the scattered signals according to modeled law in [11, 12]. As the typical coherence level in the area of fuel tanks on the interferograms mentioned is above 0.8, then in the case of the total incoherent averaging level 100 the accuracy of phase measurements is better than 5°, and the respective slant range displacement error will be less than 1 mm.

An idea about the dynamics of the scattering surfaces of the TPP3 territory during May 10, 2020 – June 03, 2020 (24 days interval covering the emergency situation) may be got from analysis of interferogram presented in upper left part of figure 3. Grey-scale variations of the tone in the range 0-255 are tied to variations of the interferometric phase difference form zero till 2π and corresponding 0-3 cm slant range variations. Below is respective amplitude image with green circle enclosing the echo-signals of 4 diesel fuel tanks. The location of the phase difference profile crossing all the 4 tanks from North-West to South-East is marked with line in the circle. Six days interferogram (June 03-09, 2020) and respective amplitude image are in the right part of the Figure. The profiles of the scattering surface displacements may be seen in figure 4.

To understand an influence of other effects like as permafrost heave in winter and frost soils thawing during warm seasons onto the tanks stability we analyzed also interferograms acquired in cold period of 2019-2020. Phase difference profiles were converted to profiles of radial displacements of the scattering surface and presented in a form of 5 plots in figure 4. Line segments in the lower part of the plot indicate the location and horizontal size of the tanks. Dashed line marks the damaged tank. According to the plot, the location of all the tanks is within 2-3 mm with respect to the supposedly stable first tank in the beginning of the plot, which was chosen as a reference target. The fact of other tanks stability is confirmed on all the observation intervals. Consequently, permafrost heave during

cold period 2019-2020 did not produce any observable displacements of the tanks eastern walls as well as adjacent portions of industrial zone.

There are some other features of interest on the interferograms which need to be commented. The dominating scattering mechanism of the industrial zone surfaces and surroundings is single scattering one. Shrub tundra covers adjacent to the industrial zone demonstrate low temporal coherence on the 24 days interval. For that reason, on the left interferogram of Fig. 3 in the lower left and fractionally in the upper right corner phase difference is obscured with noise in large extent.

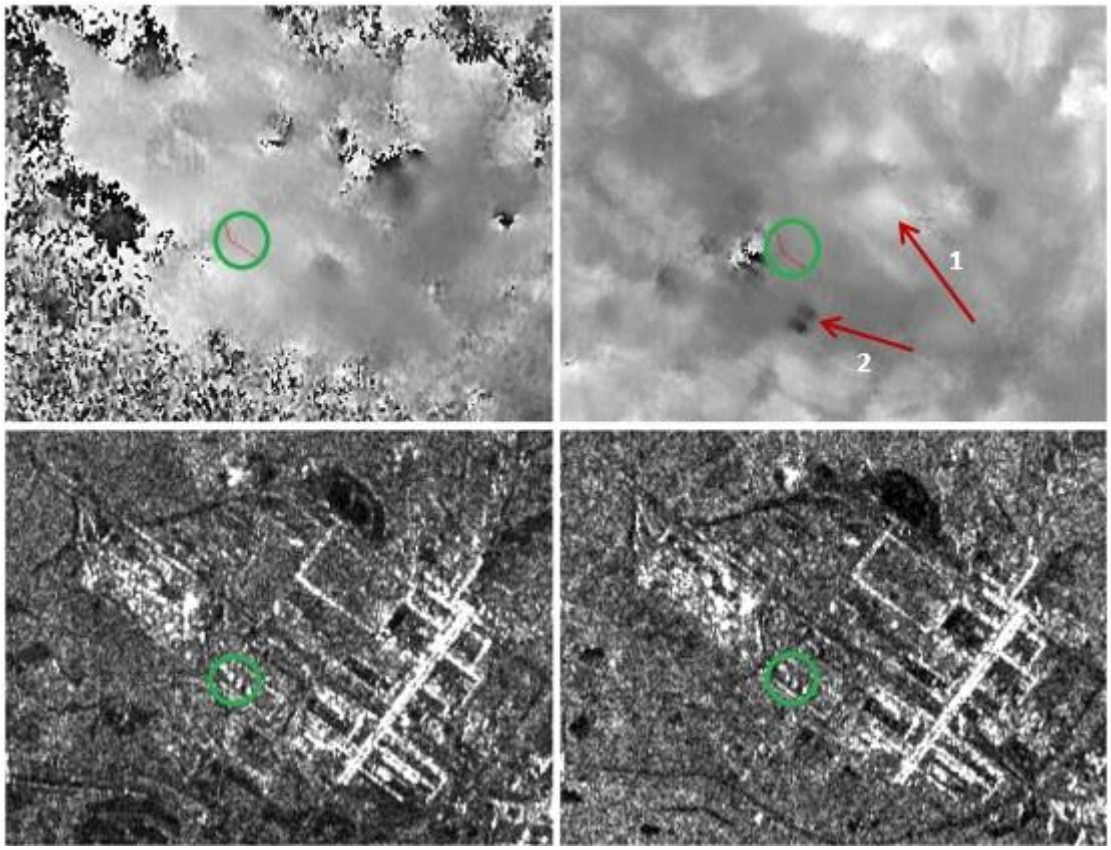

Figure 3. Fragments of interferograms (above) and Sentinel-1 images (below) for the interferometric pairs may 05- June 03,2020 (left) and June 03-09, 2020 (right).

On the right interferogram with 6 days interval the coherence is much higher; so far we may see bright spots marking 5 mm subsidence of the drying tundra pit and gley soils during 6 days. Arrow 1 marks the location of the subsiding surfaces of the elemental sulfur warehouses, slag dump and a backfilled Tumannoe Lake. Arrow 2 marks the location of spray cooling ponds visible on the radar images because of double bounce scattering from water surface and vertical pipes sprinkling the water. Seven millimeters rise of water level here during 6 days led to the decrease of the phase difference and respective darkening on the interferometric image of the ponds. The main part of the industrial zone demonstrates high stability according to almost all interferograms processed, in contrast to the surrounding tundra surface.

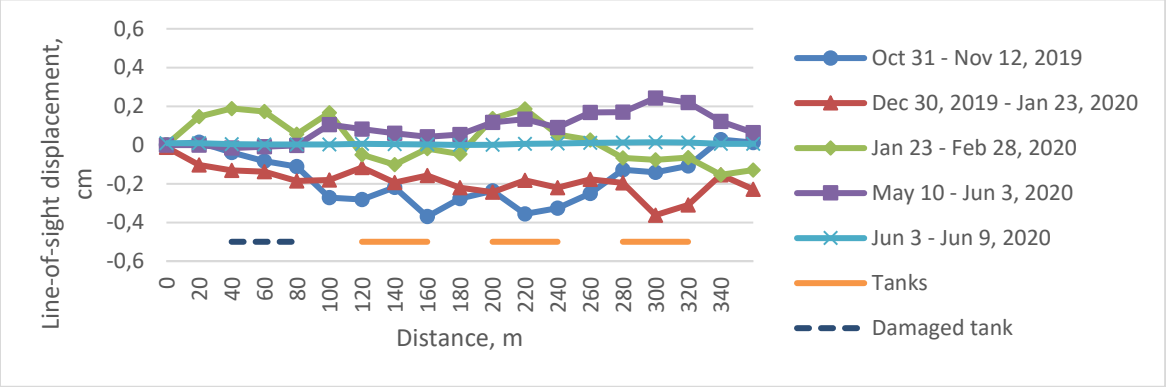

Figure 4. Profiles of the TPP-3 tanks displacements.

4. Conclusion

According to the results obtained, mutual position of all the TPP-3 tanks (their eastern walls) and adjacent territory is stable within 2-3 mm interval on all the interferograms, including the interferometric pair covering emergency event. We may suppose that the depressurization of the tank was not caused by the displacements of the TPP-3 tank scattering surfaces because of probable alteration of the permafrost state, at least starting since autumn 2019.

The work was conducted according to the State Assignment.

References

[1] Troshko K *et al*. 2020 Observation of the Ambarnaya River pollution resulting from the accident at the Norilsk Thermal Power Plant No. 3 on May 29 *Current Probl. Rem. Sens. of the Earth from Space* **17**(3) 267-74
[2] Massonnet D and Feigl K L 1998 Radar interferometry and its application to changes in the earth's surface *Rev. Geophys.* **36**(4) 441–500
[3] Hanssen R 2001 Radar Interferometry: Data Interpretation and Error Analysis (Dordrecht: Kluwer Academic)
[4] Burgmann R, Rosen P A and Fielding E J 2000 Synthetic aperture radar interferometry to measure Earth's surface topography and its deformation *Ann. Rev. of Earth and Planetary Sci.* **28** 169–209
[5] Stevens N F and Wadge G 2004 Towards operational repeat-pass SAR interferometry at active volcanoes *Natural Hazards* **33** 47–76
[6] Colesanti C and Wasowski J 2006 Investigating landslides with space-borne Synthetic Aperture Radar (SAR) interferometry *Engineering Geology* **88**(3–4) 173–99
[7] Sandwell D *et al* 2008 Accuracy and resolution of ALOS interferometry: vector deformation maps of the Father's Day intrusion at Kilauea *IEEE Trans. on Geosci. and Remote Sensing* **46**(11) 3524-34
[8] Pieraccini M *et al* 2000 Interferometric radar for remote monitoring of building deformations *Electronics Letters* **36**(6) 569-70
[9] Sousa J J *et al* 2016 Potential of C-band SAR interferometry for dam monitoring *Procedia Computer Science* **100** 1103-14
[10] Zakharova L and Zakharov A 2018 The detection of the bridges dynamics using radar interferometry technique *Current Probl. Rem. Sens. of the Earth from Space* **15**(2) 42-51
[11] Krieger G, Moreira A, Fiedler H 2007 TanDEM-X: A Satellite Formation for High Resolution SAR Interferometry, *IEEE Trans. Geosci. Remote Sensing* **45**(11) 3317–41
[12] Zebker H and Villasenor J 1992 Decorrelation in interferometric radar echoes, *IEEE Trans. Geosci. Remote Sensing* **30**(5) 950–9